KECK Geology Consortium
Learning Science Through Research
Published by the Keck Geology Consortium
Short Contributions
Keck Geology Consortium
Volume 38
May 2026
doi: 10.18277/AKRSG.2026.38.04

INVESTIGATING THE INDIAN OCEAN DIPOLE–NORTHEAST PACIFIC TELECONNECTION WITH TREE-RING CHRONOLOGIES FROM ALASKA

DEXTER C. PAKULA, Carleton College
Project Advisor: Cameron Davidson

INTRODUCTION

The skill of seasonal climatic prediction in the United States is relatively low because predictable signals are weak relative to internally generated midlatitude atmospheric variability (O'Lenic et al., 2008; Peng et al., 2012, 2013). Dominant climate modes such as the El Niño Southern Oscillation (ENSO), the Pacific Decadal Oscillation (PDO), and the Atlantic Multidecadal Variability (AMV) offer sources of predictable variability but exhibit temporal nonstationary and varying regional effects (Fernández-Castillo et al., 2025; Rohli et al., 2022). Recent studies have investigated additional climate modes and teleconnections from the tropics, such as the Indian Ocean Dipole (IOD), for sources of further predictable variability (Molteni and Brookshaw, 2024).

IOD teleconnections with the extratropics are driven by large-scale sea-surface temperature (SST) anomalies associated with an IOD event, which induce diabatic heating and excite Rossby wave trains propagating over the North Pacific (Hoskins and Karoly, 1981; McIntosh and Hendon, 2018). This influences semi-permanent pressure systems and mid-tropospheric circulation across North America and the North Atlantic (Bader and Latif, 2005; Branstator, 2002; Hu et al., 2023; Min et al., 2008). IOD teleconnections have been studied for impacts on the North Atlantic Oscillation (NAO) in early winter and climatic predictive value in Europe (Abid et al., 2023; Fereday et al., 2025; Hardi man et al., 2020; Raganato et al., 2025). Despite this attention, few studies have investigated the linkage between the IOD and North American climate (Min et al., 2008; Saji and Yamagata, 2003). One approach is to examine the climate-sensitive Northeast Pacific coastal and near-coastal tree-ring record to explore teleconnection signals from the Indian Ocean (D'Arrigo et al., 2005).

The goal of this study is to improve the understanding of the IOD–North America teleconnection using tree-ring width records from the Northeast Pacific and by utilizing the Dipole Mode Index (DMI), which characterizes the IOD. The central aims are to determine if the teleconnection signal is present in the tree-ring record from Alaska, independent of ENSO, and temporally stationary over the past few centuries. I present extended and optimized chronology network reconstructions of the DMI and the DMI with ENSO influence removed (rDMI), allowing for analysis of the teleconnection structure and the reconstruction predictive skill.

METHODS

Tree-ring Data

I utilized a dataset of 182 tree-ring width chronologies from Alaska, assembled by The College of Wooster Tree Ring Lab (WTRL). Chronologies were detrended with the signal-free approach using RCSig (Cook et al., 2017), which estimates growth-related trends while accounting for shared signals among chronologies, reducing detrending biases (Melvin and Briffa, 2008, 2014).

Chronologies were correlated with the DMI and rDMI, and those exhibiting statistically significant correlations ($p < 0.05$) for the common interval (1870-1980 CE) were retained for modeling (Fig. 1). Eighty-three chronologies were retained (Fig. 1), all of which span1835–1980 CE and are most strongly correlated

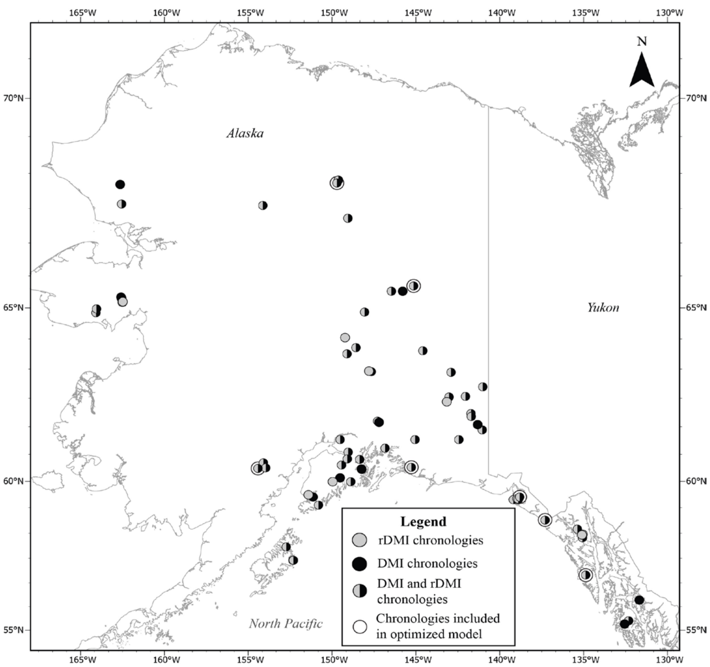

Figure 1. Locations of the tree-ring chronologies included in this study. Of the 83 total chronologies, 13 passed only the DMI screening, eight passed only the rDMI screening, and 62 passed both screenings. The chronologies marked with white circles were retained for the optimized-chronology models.

with average January–March indices (JFM; Fig. 2).

Climate Data

The SST climate data is derived from HadiSST1, which spans 1870-2025 (Rayner et al., 2003). The DMI is the SST anomaly difference between the Western Tropical Indian Ocean (WTIO; 50° E–70° E, 10° S–10° N) and the Southeastern Tropical Indian Ocean (SETIO; 90° E–110° E, 10° S–Equator; Saji et al., 1999). The Niño3.4 index represents ENSO with the average SST anomalies in the region (170° W–120° W, 5° S–5° N; Rayner et al., 2003). The rDMI was calculated by linearly regressing Niño3.4 on the DMI and retaining the residuals as a new dataset. This removes the linear portion of the influence of ENSO from the DMI.

Gridded climate datasets were used for field correlations with the principal components (PCs) derived from the chronologies that passed screening for both models. The gridded data include the HadCRUT 5.0 land and sea temperatures (Morice et al., 2021) and 500 hPa meridional wind variability and geopotential height from the NOAA 20th Century Reanalysis Version 3 monthly 2° × 2° fields (1851–2014; NOAA Physical Sciences Laboratory, 2024). These were used to explore linkages by revealing the Rossby wave structure via surface and atmospheric expressions. All climate data were acquired through the Koninklijk Nederlands Meteorologisch Instituut (2022; Trouet and Van Oldenborgh, 2013).

STATISTICAL MODELS

PC-based reconstructions were generated from the network of 83 chronologies using the principal component regression software PCreg (Cook and Krusic, n.d.). Reconstructions were calibrated over the common period between the SST data and the tree-ring data (1870–1980), modeling index values averaged over an optimal monthly interval determined from regression trials across the dendroclimatic year. Parallel reconstructions of the DMI and rDMI under the same model parameters were built to allow for isolation of the influence of ENSO on the teleconnection.

DMI Model

The DMI reconstruction was built to assess the linkage of Alaskan tree growth and Indian Ocean SST variability under the influence of ENSO. This reconstruction used 75 of the 83 chronologies and is referred to as “extended” because chronologies were included regardless of temporal stationarity (Fig. 1).

A secondary reconstruction of the DMI was built using principal component regression of a temporally stationary subset of the 75 chronologies (Fig. 1). These were identified using split-period calibration trials (1870–1925 and 1926–1980); chronologies that exhibited statistically significant correlations ($p < 0.05$) with the target index in both intervals were retained as a new dataset, and PCs were recomputed. While the extended chronology reconstruction is useful for assessing the structure of the teleconnection, the optimized one is useful for quantifying predictive skill, because it is restricted to chronologies that are consistently tuned to climate signals from the Indian Ocean throughout the modeled interval.

rDMI Model

The rDMI was reconstructed to isolate the component of the teleconnection independent of ENSO. The same processes were applied to the rDMI as were to the DMI for both extended and optimized reconstructions, though the extended reconstruction used 70 of the 83 chronologies (Fig. 1).

Model Assessment

Model assessment was conducted separately for the extended and optimized reconstructions to evaluate temporal stationarity and predictive skill, respectively. Running correlations between the reconstructions and the target index over a 30-year centered window were used to investigate the temporal stationarity of the extended models. Correlation coefficients were considered statistically significant if they exceeded a $p < 0.05$ threshold based on the two-sided Student's t-test. Predictive value of the optimized reconstructions was computed using split-period verification statistics, including the Pearson r, p-value, reduction of error (RE), and coefficient of efficiency (CE).

RESULTS

Teleconnection Signal

Principal component regression of the 182-chronology tree-ring series on the monthly DMI and rDMI over the calibration period (1870-1980) showed the strongest relationship ($R^2 > 0.28$) in January-March (JFM; Fig. 2), which restricted the final regression models to JFM (Fig. 3). A similar interval (December-May) was used for regression in D'Arrigo et al. (2005).

DMI Model

The extended JFM DMI reconstruction is shown in the upper panel of Figure 3a. The model uses 75 chronologies and five PCs to explain 39.5% of the variance in the index. The lower panel of Figure 3a is a running correlation plot, showing the 30-year averaged moving correlations throughout the modeled interval. The correlations drop below the 95% confidence interval from around 1891–1900, 1927–1932, and 1947–1952.

Five chronologies passed the criteria for the optimized

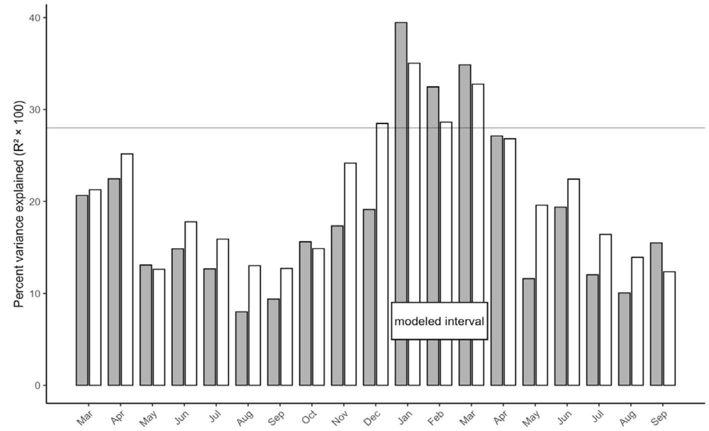

Figure 2. Monthly correlations of the model values with the corresponding index values from the DMI and rDMI between 1870 and 1980. The grey bars represent the correlations of the DMI model with the DMI, and the white bars represent the correlations of the rDMI model with the rDMI.

DMI model (Table 1), and the reconstruction used one PC to explain 40.6% of the variance in the index. Half-calibration window regression trials revealed the optimized DMI model explains 34.3% of the variance in the first period, and 24.8% in the second. The RE and CE statistics indicate robust predictive value (RE and CE > 0) across both intervals (Table 1).

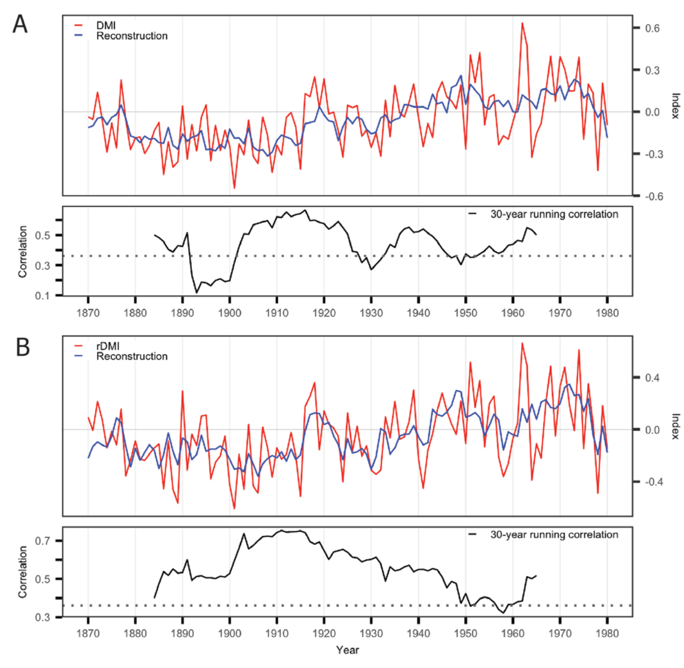

Figure 3. (A) The 75 chronology reconstruction (blue) of the JFM DMI, plotted against the index values (red). (B) The 70 chronology reconstruction (blue) of the JFM rDMI, plotted against the index values (red). Both plots include a 30-year running correlation between the model values and the index values (black). Values above the dotted line are statistically significant (p < 0.05).

Table 1. Verification statistics for optimized DMI and rDMI models

Model	Verification period	Pearson *r*	*p*	RE	CE	Durbin-Watson
DMI	1926–1980	0.510	<0.001	0.55	0.24	2.00
DMI	1870–1925	0.560	<0.001	0.66	0.29	1.90
rDMI	1926–1980	0.468	<0.001	0.41	0.19	2.07
rDMI	1870–1925	0.527	<0.001	0.50	0.23	2.03

*Verification statistics calculated using split-period calibration/verification. RE = reduction of error; CE = coefficient of efficiency.

rDMI model

The extended JFM rDMI model (Fig. 3b) uses 70 chronologies and six PCs to explain 39.7% of the variance in the index. The running correlation dips below the 95% confidence interval in the late 1950s.

Four chronologies were retained for the optimized rDMI model (Table 1). The reconstruction used one PC to explain 29.9% of the variance in the index for the whole calibration period, 32.8% in the first half, and 27.1% in the second half. The verification statistics indicate robust predictive skill (RE and CE > 0) in both intervals (Table 1).

The DMI and rDMI extended chronology reconstructions support a statistically significant linkage between tree growth in Alaska and the JFM DMI. While the extended DMI and rDMI models explain similar percentages of the variance in their target indices, the optimized models and verification statistics reveal that the DMI model possesses stronger predictive skill.

Principal Components

I computed field correlations between PC1 and PC2 (Fig. 4) of the extended DMI model and gridded climate datasets. Figure 4 is restricted to the DMI, though for both PCs, the DMI and rDMI extended models show roughly inverse patterns. PC1 shows strong negative correlations with land/SSTs in the WTIO, eastern Asia, the North Pacific, and the Atlantic tropics and extratropics. PC1's correlations with the 500 hPa meridional winds manifest as latitudinally and longitudinally alternating positive and negative fields concentrated in the Pacific. The 500 hPa geopotential height field shows a strong correlation on the coast of East Asia, and a weaker correlation to the east on the same latitude (around 30°–50°N), as well as a negative correlation field in the South Pacific.

Across all variables, the field correlations with PC1

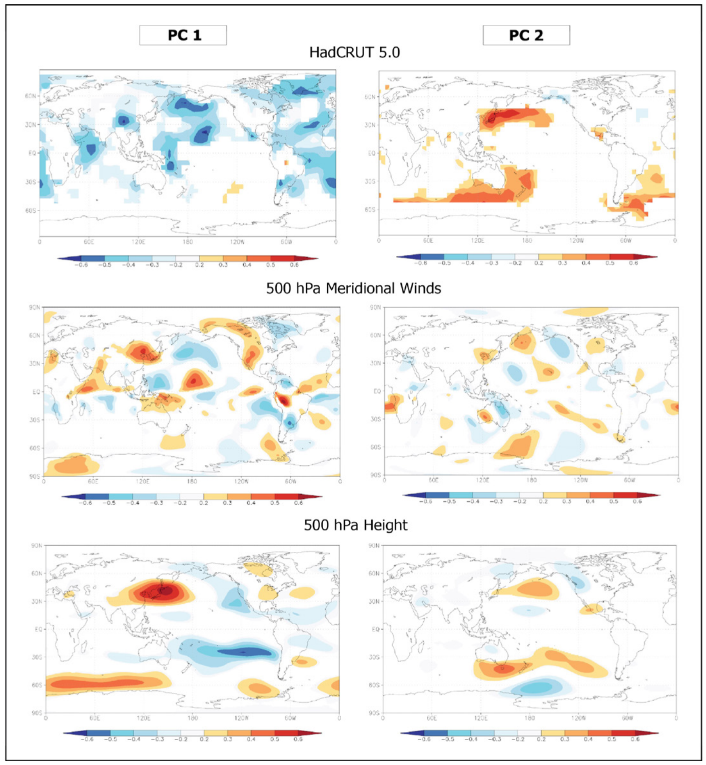

Figure 4. Extended DMI model PC1 (left) and PC2 (right) field correlations. Red indicates positive correlations, blue indicates negative correlations. The top row is correlated against land surface temperature and SST data, the middle row against 500 hPa meridional winds, and the bottom row against 500 hPa height.

are stronger and more widespread than with PC2. PC2's surface temperature correlation plot shows a positive field extending eastward from Japan. The 500 hPa meridional winds and geopotential height show weaker correlations, though similar patterns to PC1.

DISCUSSION

The reconstructions indicate a statistically significant and moderately strong teleconnection between Alaskan tree growth and the January–March (JFM) Dipole Mode Index (DMI), with the optimized models demonstrating robust predictive skill. However, the strength of the relationship may vary through time. Here, I discuss the teleconnection strength, the role of ENSO, temporal stationarity, and principal component results.

Teleconnection Strength

The extended reconstructions (Fig. 3) explain approximately 40% of the variance in the DMI and rDMI, indicating a moderate, robust relationship between Alaskan tree growth and Indian Ocean SST variability. This level of explained variance is comparable to values often obtained in dendroclimatic reconstructions of large-scale climate mode indices. Despite substantial internal variability in the midlatitude climate system, the teleconnection signal is sufficiently strong to be expressed in the tree-ring width record.

The Role of ENSO

One of the central goals of this study was to determine if a unique teleconnection exists in the absence of ENSO. Comparing the percentages of variance explained by the extended models suggests the teleconnection is not driven by ENSO; the full rDMI model explains a marginally higher percentage of the variance than the full DMI model. However, the optimized DMI model explains the highest percent variance of all models, whereas the optimized rDMI model explains the lowest percent variance; once reduced to the temporally stationary chronologies, the DMI model is strengthened, and the rDMI model is weakened. Additionally, the verification statistics reveal that the optimized DMI model is more robust than the optimized rDMI model (Table 1). ENSO likely plays a role in the teleconnection, though it is unlikely that it drives the observed linkages.

Temporal Stationarity

The sample size for the optimized models is greatly reduced from the full models (Fig. 1), indicating non-stationary tree-growth patterns with respect to the Indian Ocean Dipole (IOD). The robust RE and CE statistics partially reconcile this, though the values are lower in the latter verification interval for both models (Table 1). The running correlation plots (Fig. 3) show similar patterns–the correlations peak in the early 1900s. The DMI correlation plot shows cyclic phases of high correlations and low correlations after the early 1900s on a decadal timescale (Fig. 3a), aligning well with PDO phase changes (Mantua and Hare, 2002). The full rDMI plot shows a steady decrease without cyclicity from around 1925–1960 (Fig. 3b), aligning well with Atlantic Multidecadal Variability (AMV) phase changes (Enfield et al., 2001). Overall, the models are reasonably stationary–the teleconnection signal is rarely absent, though most of the included chronologies fail to consistently display the signal between 1870 and 1980, and large-scale climate phase changes may impact the strength of the signal.

Principal Components

The field correlations for PC1 of the DMI model show coherent, evenly spaced correlation zones (Fig. 4). The land/SST correlation plot shows two distinct negative correlation field arcs and may be the surface expression of planetary waves. In the propagation phase, Rossby waves often exhibit an arc shape prior to being guided by the jet stream and constrained to the extratropics (Branstator, 2002). The 500 hPa meridional winds show alternating zones of northerly and southerly 500 hPa winds, which is evidence of wave nodes. The 500 hPa geopotential height field plot indicates longitudinal ridge and trough topography, which is characteristic of Rossby waves, particularly in conjunction with the meridional winds pattern (Wallace and Gutzler, 1981).

The field correlations for PC2 are weaker and less widespread than those for PC1. The PC2 500 hPa meridional winds and height show a similar structure to the PC1 correlations. The PC2 land/SST field correlation exhibits a PDO-type structure, with no evidence for planetary waves. Overall, the field correlations reveal Rossby wave structure, providing additional evidence for the presence of a teleconnection linking the Indian Ocean to the Gulf of Alaska.

CONCLUSIONS

Overall, the models explain a convincing portion of the variance in the climate indices, suggesting the presence of a teleconnection linking the climate in the Northeast Pacific to the January-March (JFM) Indian Ocean Dipole (IOD). The verification statistics for the optimized models indicate that select Alaskan trees have robust predictive skill of the JFM Dipole Mode Index (DMI). The presence of a teleconnection linking the JFM DMI to the climate in the Northeast Pacific may be a valuable insight for seasonal climate prediction in North America, if the precise climatic effects can be constrained and differentiated from other Indian Ocean teleconnection signals.

ACKNOWLEDGMENTS

This material is based upon work supported by the Keck Geology Consortium and the National Science Foundation under Grant No. 2050697. I would like to thank my fellow Keck Geology Consortium researchers for many thoughtful discussions and for the time we spent together in the field, all of which helped shape this work. The ongoing support throughout the research and writing process from Greg Wiles, Cam Davidson, and Dan Maxbauer was critical for producing and refining the presented results. I am grateful for the dedication of Greg Wiles and Nick Wiesenberg to sharing the art and science of dendrochronology, and the countless lessons I learned from them both in the lab and in the field.

REFERENCES

Abid, M. A., F. Kucharski, F. Molteni, and M. Almazroui (2023), Predictability of Indian Ocean precipitation and its North Atlantic teleconnections during early winter, npj Climate and Atmo spheric Science, 6 (1), 17, doi:10.1038/s41612-023-00328-z.

Bader, J., and M. Latif (2005), North Atlantic Oscillation response to anomalous Indian Ocean SST in a coupled GCM, Journal of Climate, 18 (24), 5382–5389, doi:10.1175/JCLI3577.1.

Branstator, G. (2002), Circumglobal teleconnections, the jet stream waveguide, and the North At lantic Oscillation, Journal of Climate, 15 (14), 1893–1910, doi:10.1175/1520-0442(2002)015<1893:CTTJSW>2.0.CO;2.

Cook, E. R., and P. J. Krusic (n.d.), PcReg, Computer program, Lamont-Doherty Earth Observatory and University of Cambridge dendrochronology software archive.

Cook, E. R., P. J. Krusic, K. Peters, and T. M. Melvin (2017), Program SignalFree: RCS signal-free tree-ring standardization program.

D'Arrigo, R., R. Wilson, C. Deser, G. Wiles, E. R. Cook, R. Villalba, A. Tudhope, J. Cole, and B. Linsley (2005), Tropical–North Pacific climate linkages over the past four centuries, Journal of Climate, 18 (24), 5253–5265, doi:10.1175/JCLI3602.1.

Enfield, D. B., A. M. Mestas-Nuñez, and P. J. Trimble (2001), The atlantic multidecadal oscillation and its relation to rainfall and river flows in the continental u.s., Geophysical Research Letters, 28 (10), 2077–2080, doi:10.1029/2000GL012745.

Fereday, D. R., J. R. Knight, and A. A. Scaife (2025), Climate change alters the Indian Ocean Dipole and weakens its North Atlantic teleconnection, Communications Earth & Environment, 6 (1), 152, doi:10.1038/s43247-025-02131-5.

Fernández-Castillo, P., T. Losada, B. Rodríguez-Fonseca, D. García-Maroto, E. Mohino, and L. Durán (2025), Multidecadal variability of the ENSO early-winter teleconnection to Europe and implications for seasonal forecasting, npj Climate and Atmospheric Science, 8 (1), 272, doi: 10.1038/s41612-025-01160-3.

Hardiman, S. C., N. J. Dunstone, A. A. Scaife, D. M. Smith, J. R. Knight, P. Davies, M. Claus, and R. J. Greatbatch (2020), Predictability of European winter 2019/20: Indian Ocean Dipole impacts on the NAO, Atmospheric Science Letters, 21 (12), e1005, doi:10.1002/asl.1005.

Hoskins, B. J., and D. J. Karoly (1981), The steady linear response of a spherical atmosphere to thermal and orographic forcing, Journal of the Atmospheric Sciences, 38 (6), 1179–1196, doi: 10.1175/1520-0469(1981)038<1179:TSLROA>2.0.CO;2.

Hu, Z.-Z., A. Kumar, B. Jha, M. Chen, and W. Wang (2023), The tropical Indian Ocean matters for U.S. winter precipitation variability and predictability, Environmental Research Letters, 18 (7), doi:10.1088/1748-9326/ace06e.

Koninklijk Nederlands Meteorologisch Instituut (KNMI) (2022), KNMI Climate Explorer, Available at https://climexp.knmi.nl/start.cgi, accessed 17 November 2025.

Mantua, N. J., and S. R. Hare (2002), The pacific decadal oscillation, Journal of Oceanography, 58 (1), 35–44, doi:10.1023/A:1015820616384.

McIntosh, P. C., and H. H. Hendon (2018), Understanding Rossby wave trains forced by the Indian Ocean Dipole, Climate Dynamics, 50 (7-8), 2783–2798, doi:10.1007/s00382-017-3771-1.

Melvin, T. M., and K. R. Briffa (2008), A "signal-free" approach to dendroclimatic standardisation, Dendrochronologia, 26 (2), 71–86, doi:10.1016/j.dendro.2007.12.001.

Melvin, T. M., and K. R. Briffa (2014), CRUST: Software for the implementation of regional chronol ogy standardisation: Part 2. Further RCS options and recommendations, Dendrochronologia, 32 (4), 343–356, doi:10.1016/j.dendro.2014.07.008.

Min, J., Q. Zhou, N. Liu, Q. Gao, and Z. Guan (2008), Teleconnection mode between IOD and northern hemisphere tropospheric circulation and its mechanism, Meteorology and Atmospheric Physics, 100 (1), 207–215, doi:10.1007/s00703-008-0304-9.

Molteni, F., and A. Brookshaw (2024), Indian Ocean teleconnections to the northern extra-tropics, ECMWF Technical Memorandum 923, European Centre for Medium-Range Weather Forecasts, Reading, UK.

Morice, C. P., J. J. Kennedy, N. A. Rayner, J. P. Winn, E. Hogan, R. E. Killick, R. J. H. Dunn, T. J. Osborn, P. D. Jones, and I. R. Simpson (2021), An updated assessment of near-surface temperature change from 1850: The HadCRUT5 data set, Journal of Geophysical Research: Atmospheres, 126, e2019JD032,361, doi:10.1029/2019JD032361.

NOAA Physical Sciences Laboratory (2024), NOAA 20th century reanalysis version 3 (2° × 2°, 1851–2014), accessed 15 February 2026.

O'Lenic, E. A., D. A. Unger, M. S. Halpert, and K. S. Pelman (2008), Developments in operational long-range climate prediction at CPC, Weather and Forecasting, 23 (3), 496–515.

Peng, P., A. Kumar, M. S. Halpert, and A. G. Barnston (2012), An analysis of CPC's operational 0.5-month lead seasonal outlooks, Weather and Forecasting, 27 (4), 898–917.

Peng, P., A. G. Barnston, and A. Kumar (2013), A comparison of skill between two versions of the NCEP Climate Forecast System (CFS) and CPC's operational short-lead seasonal outlooks, Weather and Forecasting, 28 (2), 445–462.

Raganato, A., M. A. Abid, and F. Kucharski (2025), The combined link of the Indian Ocean Dipole and ENSO with the North Atlantic–European circulation during early boreal winter in reanalysis and the ECMWF SEAS5 Hindcast, Journal of Climate, 38 (2), 445–460, doi: 10.1175/JCLI-D-23-0703.1.

Rayner, N. A., D. E. Parker, E. B. Horton, C. K. Folland, L. V. Alexander, D. P. Rowell, E. C. Kent, and A. Kaplan (2003), Global analyses of sea surface temperature, sea ice, and night marine air temperature since the late nineteenth century, Journal of Geophysical Research: Atmospheres, 108 (D14), doi:10.1029/2002JD002670.

Rohli, R. V., G. A. Snedden, E. R. Martin, and K. L. DeLong (2022), Impacts of ocean-atmosphere teleconnection patterns on the south-central United States, Frontiers in Earth Science, Volume 10 - 2022, doi:10.3389/feart.2022.934654.

Saji, N. H., and T. Yamagata (2003), Possible impacts of the Indian Ocean dipole mode events on global climate, Climate Research, 25 (2), 151–169.

Trouet, V., and G. J. Van Oldenborgh (2013), KNMI Climate Explorer: A web-based research tool for high-resolution paleoclimatology, Tree-Ring Research, 69 (1), 3–13, doi:10.3959/1536-1098-69.1.3.

Wallace, J. M., and D. S. Gutzler (1981), Teleconnections in the geopotential height field dur ing the northern hemisphere winter, Monthly Weather Review, 109 (4), 784–812, doi:10.1175/1520-0493(1981)109<0784:TITGHF>2.0.CO;2.